

Revisiting Inert Doublet Model Parameters

Hamza Abouabid,^{1,*} Abdesslam Arhrib,^{1,†} Ayoub Hmissou,^{2,‡} and Larbi Rahili^{2,§}

¹*Département de Mathématiques, Faculté des Sciences et Techniques,*

Université Abdelmalek Essaadi, B. 416, Tangier, Morocco.

²*Laboratory of Theoretical and High Energy Physics,*

Faculty of Science, Ibnou Zohr University, B.P 8106, Agadir, Morocco.

(Dated: February 2, 2024)

In this study, we aim to see how much the actual measurement of the Z+photon and di-photon signal strength, $\mu_{\gamma\gamma}$ and $\mu_{\gamma Z}$, could influence the allowed parameter space of the Inert Doublet Model (IDM), and to what extent such measurement can be aligned with the latest bound from XENON1T experiment on the spin-independent dark-matter-nucleon scattering cross-section. Also, by considering the new embedded scalars in the IDM (i.e., H , A and H^\pm), a wide investigation of the one-loop radiative corrections to the trilinear Higgs coupling hhh has been made in the light of the previous measurements

I. INTRODUCTION

Following the discovery of the Higgs boson at the Large Hadron Collider (LHC) [1, 2], the standard model (SM) of particle physics was crowned with great success and highly accurate predictions to date. The LHC program has already performed so far several precise measurements of the Higgs coupling to SM particles. These measurements demonstrate that the SM works well in explaining these observed phenomena at the electroweak scale. Moreover, SM has no answer to a few problems like non-zero neutrino masses, dark matter (DM) and nongravitational interactions, etc. This has prompted the search for new physics (NP) beyond the Standard Model (BSM) by extending the SM to contain extra: real or complex singlets, doublets, triplets higgs fields.

* hamza.abouabid@gmail.com

† aarhrib@gmail.com

‡ ayoub1hmissou@gmail.com

§ l.rahili@uiz.ac.ma/rahililarbi@gmail.com

The Inert Doublet Model (IDM) [3–5] constitutes a simple and a phenomenologically interesting extension of the SM Higgs sector which features a DM candidate. It is a version of the 2 Higgs Doublet Model (2HDM) with an exact \mathbb{Z}_2 symmetry, consisting of adding an inert scalar doublet H_2 to the SM Higgs doublet H_1 . The doublet H_2 is odd under the new discrete \mathbb{Z}_2 symmetry and does not couple with fermions, does not develop a vacuum expectation value (VEV). Such modified version of the 2HDM with an exact \mathbb{Z}_2 symmetry is motivated by having a potential source of a weakly interacting massive particle (WIMP) as well as a possible explanation of the observed excess of cosmic-ray positrons [6, 7].

The purpose of this paper is to investigate the effect of the current measurement of the di-photon ($\mu_{\gamma\gamma}$) and the recent Z-photon ($\mu_{\gamma Z}$) signal strengths on the IDM parameter space. Since these 2 observables are sensitive only to the charged scalar contributions, one can use them to set a constraint on the coupling hH^+H^- once the charged scalar boson mass is fixed. In the numerical scan, we will take into consideration all theoretical constraints on the scalar sector of the model as well as LHC experimental measurement such $\mu_{\gamma\gamma}^{exp}$ and $\mu_{Z\gamma}^{exp}$ and the invisible decay of the SM higgs. In addition, an update on the effects of the extra scalars of the IDM onto the radiative corrections to the triple Higgs coupling hhh at the one-loop level is presented. We also examine to what extent such measurements can be consistent with the latest bound from XENON1T experiment on the spin-independent dark-matter-nucleon scattering cross-section.

The paper is structured as follows. In Sec. II we review the details of the IDM including its scalar potential and the corresponding constraints. In section III, a detailed look at the signal strength $h \rightarrow \gamma\gamma$ and $h \rightarrow Z\gamma$ measurements is considered and the allowed parameter space for the parameters involved is quantified. In section IV, we present our result for the triple higgs coupling hhh in several scenario and show the consistency of our scan with the bound from XENON1T experiment and conclude in Sec. V.

II. THE CANONICAL INERT DOUBLET MODEL

A. Overview

The IDM is a slightly extended version of the SM that preserves its heritage in fermion and gauge bosons sectors at tree level. Thus, an additional doublet Φ_2 without a VEV was

incorporated into the SM Higgs sector, and considering the fact that general \mathbb{Z}_2 -invariance is imposed, the particles in the inert doublet Φ_2 are odd while the remaining fields are even under \mathbb{Z}_2 . The physical parametrization of the scalar doublets has the form

$$H_1 = \begin{pmatrix} G^+ \\ \frac{1}{\sqrt{2}}(v + h + iG) \end{pmatrix} \text{ and } H_2 = \begin{pmatrix} H^+ \\ \frac{1}{\sqrt{2}}(S + iA) \end{pmatrix}, \quad (1)$$

The most general (dimension 4) $SU(2)_L \times U(1)_Y$ gauge invariant scalar potential with an exact \mathbb{Z}_2 symmetry takes the following form:

$$\begin{aligned} V = & \mu_{11}^2 H_1^\dagger H_1 + \mu_{22}^2 H_2^\dagger H_2 + \eta_1 \left(H_1^\dagger H_1 \right)^2 + \eta_2 \left(H_2^\dagger H_2 \right)^2 \\ & + \eta_3 \left(H_1^\dagger H_1 \right) \left(H_2^\dagger H_2 \right) + \eta_4 \left(H_1^\dagger H_2 \right) \left(H_2^\dagger H_1 \right) \\ & + \frac{1}{2} \eta_5 \left[\left(H_1^\dagger H_2 \right)^2 + \left(H_2^\dagger H_1 \right)^2 \right], \end{aligned} \quad (2)$$

where μ_{11}^2 and μ_{22}^2 are mass terms and $\eta_{1,2,3,4,5}$ are quartic couplings. Electroweak symmetry is broken when H_1 gets its VEV $\langle H_1 \rangle_0 = v$ GeV while H_2 stays with a vanishing VEV. G^\pm and G are the charged and neutral Goldstone bosons respectively, which are absorbed by the longitudinal component of W^\pm and Z to acquire their masses. The Higgs spectrum of the model contains: *i*) the SM Higgs boson h and a neutral scalars boson S which are defined as scalars transforming to CP symmetry in a even way, *ii*) a pseudo-scalar field, A , changing odd under CP symmetry and *iii*) the fields H^\pm that are the charged scalar bosons.

The scalar bosons masses are given by:

$$m_h^2 = 2\eta_1 v^2 = -2\mu_{11}^2, \quad (3)$$

$$m_S^2 = \mu_{22}^2 + \eta_L v^2, \quad (4)$$

$$m_A^2 = \mu_{22}^2 + \eta_S v^2, \quad (5)$$

$$m_{H^\pm}^2 = \mu_{22}^2 + \frac{1}{2}\eta_3 v^2, \quad (6)$$

where the new expressions $\eta_{L,S}$ are as follows

$$\eta_L = \frac{1}{2}(\eta_3 + \eta_4 + \eta_5) \text{ , } \eta_S = \frac{1}{2}(\eta_3 + \eta_4 - \eta_5). \quad (7)$$

Moreover, the splitting among the neutral, charged scalar masses as well as the μ_{22}^2 might

be expressed by

$$\Delta m_0^2 = m_S^2 - m_A^2 = \eta_5 v^2, \quad (8)$$

$$\Delta m_1^2 = m_S^2 + m_A^2 - 2m_{H^\pm}^2 = \eta_4 v^2, \quad (9)$$

$$\Delta m_2^2 = m_{H^\pm}^2 - \mu_{22}^2 = \frac{1}{2}\eta_3 v^2. \quad (10)$$

which could be worthwhile manner to give viable values for the particular quartic couplings η_3 , η_4 and η_5 . As it can be seen from above, η_5 can be determined from the splitting between the square of S and A masses. The IDM Higgs sector is thus described by the following six parameters, which we choose to be

$$\mathcal{P} = \{\mu_{22}^2, \eta_2, m_h, m_S, m_A, m_{H^\pm}\} \quad (11)$$

in which the scalar field h fully mimics the SM Higgs boson in mass and couplings with fermionic and gauge bosonic fields. For the self-Higgs coupling hhh , as for its coupling to the charged scalar bosons, both can be derived at the tree-level from the scalar potential in Eq.(2). They read,

$$\eta_{hhh} = -3m_h^2/v, \quad (12)$$

$$\eta_{hH^\pm H^\mp} = \frac{2}{v} (\mu_{22}^2 - m_{H^\pm}^2) = -\eta_3 v \quad (13)$$

Here, as clearly indicated by Eq.(13), the coupling $hH^\pm H^\mp$ is directly related to the quartic coupling η_3 , which is in turn related to the splitting between the charged scalar boson mass square and μ_{22}^2 : $(\mu_{22}^2 - m_{H^\pm}^2)$. Furthermore, the value of the leading order self coupling η_{hhh} is fixed by the experimental measurement of the Higgs masse m_h .

B. Theoretical and Experimental Constraints

In the following, we sum up all theoretical constraints that must be imposed on the scalar sector, for the IDM to be consistent with the principles of electroweak symmetry breaking. Firstly, the unitarity constraints puts bounds on the amplitude of partial waves [8], which in turn curtail the values of the coupling constants. The latter go into the composition of

the \mathcal{S} -scattering matrix eigenvalues given by

$$\begin{aligned}
e_{1,2} &= \eta_3 \pm \eta_4, \quad e_{3,4} = \eta_3 \pm \eta_5 \\
e_{5,6} &= \eta_3 + 2\eta_4 \pm 3\eta_5 \\
e_{7,8} &= -\eta_1 - \eta_2 \pm \sqrt{(\eta_1 + \eta_2)^2 + \eta_4^2} \\
e_{9,10} &= -3\eta_1 - 3\eta_2 \pm \sqrt{9(\eta_1 - \eta_2)^2 + (2\eta_3 + \eta_4)^2} \\
e_{11,12} &= -\eta_1 - \eta_2 \pm \sqrt{(\eta_1 - \eta_2)^2 + \eta_5^2}
\end{aligned} \tag{14}$$

which must all be below 8π . Pursuant to such requirement, a compact constraint on $\eta_{1,2}$ stands out to be : $\eta_{1,2} \leq 4\pi/3$. We also recall that the potential is also perturbative, so we will impose that all the quartic couplings in Eq.(2) to be $|\eta_i| \leq 8\pi$.

Secondly, in order to have one minimum value, the scalar potential of the IDM model must be bounded from below in all directions of the space-field when the scalar fields become quite large. This corresponds to :

$$\begin{aligned}
\eta_1 > 0, \quad \eta_2 > 0, \quad \eta_3 + 2\sqrt{\eta_1\eta_2} > 0 \\
\text{and } \eta_3 + \eta_4 - |\eta_5| > 2\sqrt{\eta_1\eta_2}
\end{aligned} \tag{15}$$

Similarly, a sufficient but not necessary condition to get neutral charge-conserving vacuum, should be imposed to the potential [9]:

$$\eta_4 \leq |\eta_5| \tag{16}$$

while the following constraints

$$m_h^2, m_S^2, m_A^2, m_{H^\pm}^2 > 0 \quad \text{and} \quad v^2\sqrt{\eta_1\eta_2} + \mu_{22}^2 > 0 \tag{17}$$

are vital to having an inert vacuum [9].

Thirdly, the quantum corrections parameterized by the oblique parameters S, T and U [10], make it possible to scrutinize the NP in the electroweak domain, and, accordingly, their effects on the W and Z bosons self energies may also restrain the IDM space parameter (see Ref.[5] for the analytic S and T formulas in the IDM). Those parameters are mainly sensitive to the above splitting between the scalar states, and when fixing ΔU at zero, their allowable values, according to the latest global fit of electroweak precision data read [11]:

$$\Delta S = -0.01 \pm 0.07, \quad \Delta T = 0.04 \pm 0.06 \tag{18}$$

Overall, throughout our study, such oblique parameters are performed at 2σ using the PDG results, and other collider constraints [4, 12–16] that satisfy lower bounds on the new scalar bosons masses have been considered.

Experimentally, constraints from direct searches at LEP, adapted from the production neutralinos and charginos in the framework of the Minimal Supersymmetric Standard Model, bound the scalar masses as follows [17, 18] :

$$m_{H^\pm} > 80 \text{ GeV}, \quad \max(m_A, m_S) > 100 \text{ GeV}, \quad (19)$$

$$m_A + m_S > m_Z \quad \text{and} \quad m_A + m_{H^\pm} > m_W \quad (20)$$

Additionally, to examine more widely the IDM space parameter, we evaluate the signal strength, defined as,

$$\mu_{V\gamma} = \frac{\sigma(pp \rightarrow h)}{\sigma^{SM}(pp \rightarrow h)} \times \frac{Br(h \rightarrow V\gamma)}{Br(h_{SM} \rightarrow V\gamma)}, \quad \text{with } V = \gamma \text{ or } Z, \quad (21)$$

and compare it to the experiment measurement values. Signal strengths for both decay modes have been analyzed at 13 TeV center of mass energy. The best fit values for the $h \rightarrow \gamma\gamma$ decay mode, as reported by ATLAS [19] and CMS [20], are respectively given by:

$$\mu_{\gamma\gamma}^{\text{ATLAS}} = 1.04^{+0.10}_{-0.09}, \quad (22)$$

$$\mu_{\gamma\gamma}^{\text{CMS}} = 1.12^{+0.09}_{-0.09}. \quad (23)$$

For the $h \rightarrow \gamma Z$ decay mode, CMS [21] reports a best fit value of:

$$\mu_{Z\gamma}^{\text{CMS}} = 2.4 \pm 0.9. \quad (24)$$

Moreover, with the upcoming HL-LHC project, increasing sensitivity is expected to boost the corresponding forward-looking measurements, potentially achieving high accuracy of [22]:

$$\mu_{\gamma\gamma}^{\text{HL-LHC}} = 1 \pm 0.04 \quad \text{and} \quad \mu_{Z\gamma}^{\text{HL-LHC}} = 1 \pm 0.23. \quad (25)$$

However, after extensive work, ATLAS and CMS combined their data and found the first proof of the $h \rightarrow Z\gamma$ decay [23], with a statistical significance of 3.4 standard deviation. The observed signal strength is: $\mu_{Z\gamma}^{\text{exp}} = 2.2 \pm 0.7$ which is consistent with the SM theoretical expectation within 1.9 standard deviations.

Note that in the IDM, the signal strength of $h \rightarrow \gamma\gamma$ and $h \rightarrow Z\gamma$ reduces to the ratio of

the corresponding Branching ratio normalized to the SM value. This is mostly caused by the fact that, at the leading order, $\sigma(gg \rightarrow h)$ is the same in both the IDM and SM.

The above LHC constraints on the signal strength $\mu_{\gamma\gamma}^{exp}$ are $\mu_{Z\gamma}^{exp}$ together with the invisible decay constraints are the only ones to consider since the Higgs is SM like, all Higgs production cross sections as well as Higgs decay are exactly as in the SM.

III. $h \rightarrow \gamma\gamma$ AND $h \rightarrow Z\gamma$ IN THE IDM

At one loop level, the di-photon Higgs decay (together with photon+Z boson decay scheme) could be mediated by the newly charged scalar boson, H^\pm in addition to the SM contribution dominated by the W loops. The corresponding decay widths are given explicitly by [24–28], and take the form

$$\Gamma(h \rightarrow \gamma\gamma) = \frac{G_F \alpha^2 m_h^3}{128 \sqrt{2} \pi^3} \left| \sum_f \underbrace{Q_f^2 N_c A_{\frac{1}{2}}^{\gamma\gamma}(\tau_f)}_{C_{top}} + \underbrace{A_1^{\gamma\gamma}(\tau_W)}_{C_W} - \underbrace{\frac{m_W}{g m_{H^\pm}^2} \eta_{hH^\pm H^\mp} A_0^{\gamma\gamma}(\tau_{H^\pm})}_{C_{H^\pm}} \right|^2 \quad (26)$$

$$\begin{aligned} \Gamma(h \rightarrow Z\gamma) = & \frac{G_F^2 \alpha m_h^3 m_W^2}{64 \pi^4} \left(1 - \frac{m_Z^2}{m_h^2} \right) \left| \sum_f \underbrace{\frac{N_c Q_f \hat{v}_f}{c_w} A_{\frac{1}{2}}^{\gamma Z}(\tau_f, \lambda_f)}_{C_{top}} + \underbrace{A_1^{\gamma Z}(\tau_W, \lambda_W)}_{C_W} \right. \\ & \left. + \underbrace{\frac{v v_{H^\pm}}{2 m_{H^\pm}} \eta_{hH^\pm H^\mp} A_0^{\gamma Z}(\tau_{H^\pm})}_{C_{H^\pm}} \right|^2 \end{aligned} \quad (27)$$

with $\hat{v}_f = 2I_f^3 - 4Q_f s_W^2$ and $v_{H^\pm} = \frac{2c_W^2 - 1}{c_W}$. Here N_c is the color factor $N_c = 3(1)$ for quarks(leptons) and Q_f stands for the electric charge of a particle in the loop. α is the fine-structure constant. The $A_{1/2}^{VV}$, with $VV \equiv \gamma\gamma, \gamma Z$, (for the fermions, $f = t, b, \tau$) as well as the A_1^{VV} (for the W boson) and A_0^{VV} (for the charged scalars, H^\pm) are three dimensionless form factors for spin-1/2, spin-1 and spin-0 particles, which can be expressed using the Passarino-Veltman functions [29]. Furthermore, considering Eqs.(6)-(13), it is obvious that m_{H^\pm} , μ_{22} or η_3 are the relevant keys that could diminish or enhance the IDM prediction of $\Gamma(h \rightarrow \gamma\gamma)$ and $\Gamma(h \rightarrow Z\gamma)$ compared to the SM one. Since the charged Higgs contribution is proportional to hH^+H^- coupling which is in turn proportional to η_3 , depending on the sign of η_3 the charged Higgs contribution could be either constructive or destructive with the dominant W loop contributions. Furthermore, it is crucial to highlight that two-loop corrections to the Higgs di-photon decay have been carried out within the IDM, allowing

reliable comparisons between theoretical predictions and experimental results. For more details, we refer the reader to Ref.[30].

The model parameters in Eq.(11) are randomly scanned within the following ranges:

$$\begin{aligned} m_h &= 125.09 \text{ GeV} \\ \eta_2 &\in [0, 4\pi/3] \quad , \quad \mu_{22}^2 \in [-10^5, 10^5] \quad (\text{GeV}^2) \\ m_{S,A} &\in [50, 500] \quad (\text{GeV}) \quad , \quad m_{H^\pm} \in [80, 500] \quad (\text{GeV}) \end{aligned} \quad (28)$$

In Figure.1, we illustrate a scatter plot comparing the squared moduli of the various contributions in Eqs.(26-27) without regard for any theoretical constraints on the scalar potential parameters (for the fermionic one, we have drawn only the top quark contribution). As it

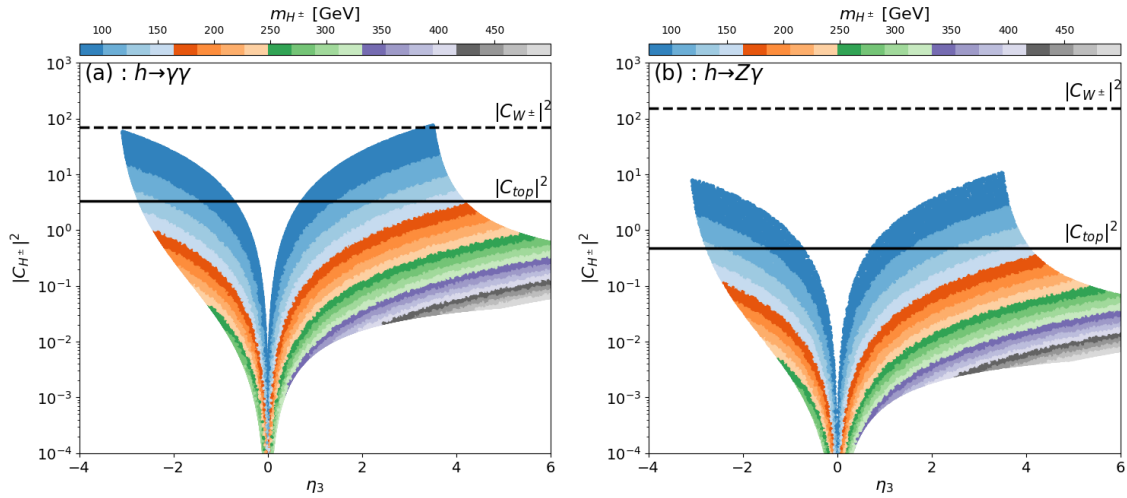


FIG. 1. The squared moduli of charged scalar boson contribution C_{H^\pm} for $h \rightarrow \gamma\gamma$ (left) and $h \rightarrow Z\gamma$ (right) amplitudes, as a function of η_3 coupling. The top and W^\pm contributions are shown for comparison. The color coding exhibits the charged scalar boson mass m_{H^\pm} . None of the theoretical or experimental constraints are applied.

can be observed, the diagrams mediated by internal vectorial bosons (W^\pm) have the most expressive contribution compared to the top quark, either for $h \rightarrow \gamma\gamma$ (Figure.1-(a)) or $h \rightarrow Z\gamma$ (Figure.1-(b)). Nevertheless, the charged scalar boson contribution is non-negligible, and could contribute significantly by some few orders of magnitude. It is obvious that for small $\eta_3 \approx 0$, $|C_{H^\pm}|^2$ is very suppressed. While for large value of η_3 together with light charged scalar boson mass in the range $[80, 150]$ GeV one can see that $|C_{H^\pm}|^2$ could be between $|C_{top}|^2$ and $|C_{W^\pm}|^2$, and can get to $|C_{W^\pm}|^2$ value for the $\gamma\gamma$ mode as it can be seen from

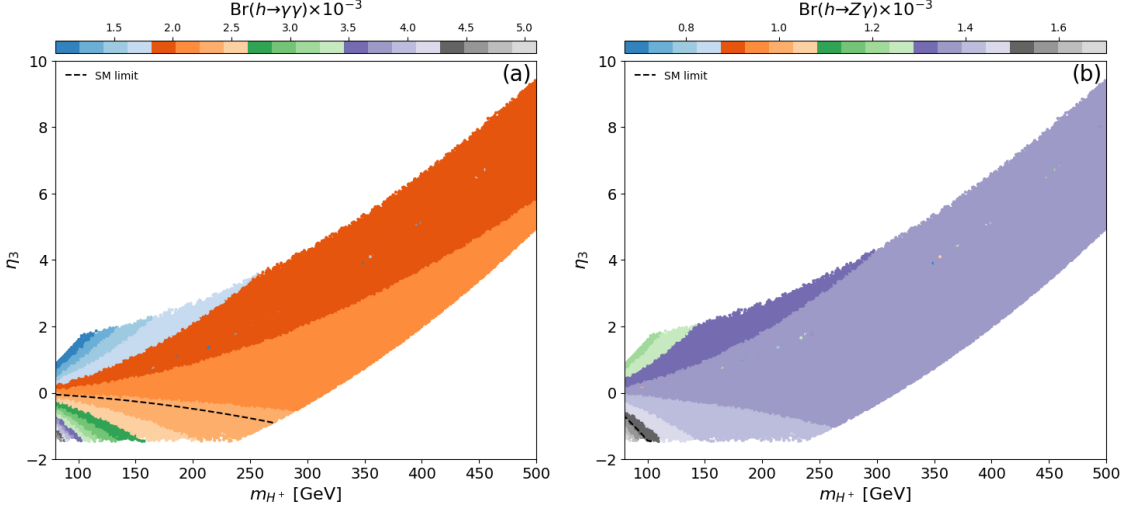


FIG. 2. Branching ratios: $\text{Br}(h \rightarrow \gamma\gamma)$ (left panel) and $\text{Br}(h \rightarrow Z\gamma)$ (right panel) as a function of m_{H^\pm} and the coupling η_3 . Theoretical constraints as well as LEP requirements are applied.

Figure.1-(a). For heavier charged scalar boson ≥ 150 GeV, its contribution drops below $|C_{top}|^2$. However, such contribution could be either constructive or destructive with the W loops.

Figure.2 could promote the aforementioned interference. Indeed, by considering the LEP constraints, we illustrate $\text{Br}(h \rightarrow \gamma\gamma)$ (left) and $\text{Br}(h \rightarrow Z\gamma)$ (right) as a function of m_{H^\pm} and η_3 . For $\text{Br}(h \rightarrow \gamma\gamma)$, it is clear that there is a large area of parameter space where the branching ratio is smaller than the SM value and this is because of the destructive interference between the W^\pm and H^\pm loops. One can also see a small region with negative η_3 and rather light charged scalar boson m_{H^\pm} where $\text{Br}(h \rightarrow \gamma\gamma)$ is greater than the SM value, and this is due to the constructive interference between W^\pm and H^\pm loops.

For the $Z\gamma$ decay mode, it can be observed that, except for a very small region with $\eta_3 < 0$ and charged scalar boson masses less than 100 GeV, the $\text{Br}(h \rightarrow Z\gamma)$ is below the SM value on the whole. This region corresponds to constructive interference between the SM Higgs and the charged scalar loops. Conversely, in the opposite case, there is a large area in the charged scalar boson mass and η_3 parameter space where the $\text{Br}(h \rightarrow Z\gamma)$ is smaller than the SM value.

IV. RESULTS AND DISCUSSION

In this section, we illustrate the result of our scan both for the triple coupling hhh as well as the consistency of our result with XENON1T experiment on the spin-independent dark-matter-nucleon scattering cross-section. To address that purpose, we explore some numerical consequences distinguishing between two cases:

- Degenerate case where $m_S = m_A = m_{H^\pm} = m_\Phi$, in other words $\Delta m_0 = \Delta m_1 = 0$, that will enable us to avoid electroweak precision observables (EMPO) constraints in IDM.
- Quasi-degenerate case where $m_S \neq m_A = m_{H^\pm}$ and $m_S \leq m_h/2$.

and whose only those that obey the boundary parameters allowed by the limitations of the previous theoretical as well as the experimental constraints are survived.

A. Radiative Corrections to hhh

In this section, we will illustrate the impact of $\mu_{\gamma\gamma}^{exp}$ measurement on the trilinear coupling η_{hhh} within the IDM. The latter has been the subject of several studies BSM such as: MSSM [31], 2HDM [32] and the IDM [33]. They have applied renormalization techniques to this issue and show its sensitivity to the NP effects BSM. Here, with the aim of addressing the IDM towards such measurements, we revisit the additional contribution to the following process,

$$h(q) \rightarrow h(k_1) + h(k_2) \tag{29}$$

where q (resp. k_1 and k_2) denotes the 4-momenta of the incoming particle satisfying off shell condition $q^2 \neq m_h^2$ (resp. the 4-momenta of the outgoing particles satisfying on shell condition $k_1^2 = k_2^2 = m_h^2$), is calculated from the Feynman diagrams depicted in Figure.3

As is also being demonstrated in [33], the contribution of the IDM is purely bosonic backed by the h_{125} Higgs boson couplings to the new inert scalars. Hence, the corresponding

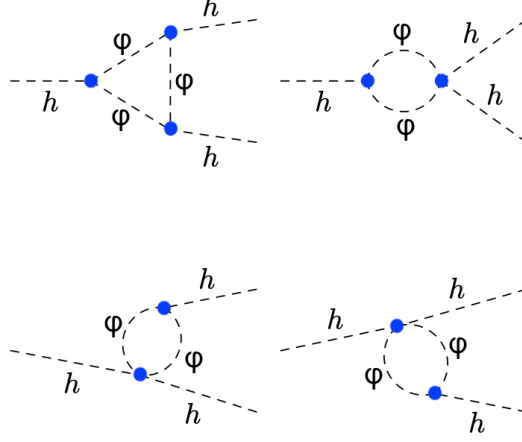


FIG. 3. Diagrams contributing, at one-loop, to the radiative corrections of the trilinear coupling η_{hhh} in the IDM. The φ stands for any scalar S , A and H^\pm .

amplitude, is given by

$$\begin{aligned}
 \Gamma_{hhh}^{loop}(q^2, m_\Phi^2) &= \frac{\eta_3^2 m_W s_W}{8e\pi^2} \left(B_0(q^2, m_{H^\pm}^2, m_{H^\pm}^2) + 2B_0(m_h^2, m_{H^\pm}^2, m_{H^\pm}^2) \right. \\
 &\quad \left. + \frac{2\eta_3 m_W^2 s_W^2}{\pi\alpha} C_0(q^2, m_h^2, m_h^2, m_{H^\pm}^2, m_{H^\pm}^2, m_{H^\pm}^2) \right) \\
 &\quad + \frac{(\eta_3 + \eta_4 + \eta_5)^2 m_W s_W}{16e\pi^2} \left(B_0(q^2, m_S^2, m_S^2) + 2B_0(m_h^2, m_S^2, m_S^2) \right. \\
 &\quad \left. \times \frac{2(\eta_3 + \eta_4 + \eta_5) m_W^2 s_W^2}{\pi\alpha} C_0(q^2, m_h^2, m_h^2, m_S^2, m_S^2, m_S^2) \right) \\
 &\quad + \frac{(\eta_3 + \eta_4 - \eta_5)^2 m_W s_W}{16e\pi^2} \left(B_0(q^2, m_A^2, m_A^2) + 2B_0(m_h^2, m_A^2, m_A^2) \right. \\
 &\quad \left. \times \frac{2(\eta_3 + \eta_4 - \eta_5) m_W^2 s_W^2}{\pi\alpha} C_0(q^2, m_h^2, m_h^2, m_A^2, m_A^2, m_A^2) \right) \quad (30)
 \end{aligned}$$

with B_0 and C_0 are the Passarino-Veltman functions [29] is not UV finite, it was important to add the corresponding counter-term, $\delta\Gamma_{hhh}^{loop}$, and evaluate them by calculating the necessary and sufficient renormalization constants. For more details, we refer the reader to [33].

In line with our purpose in this study, we redefine a ratio that involves the previous quantities as,

$$\Delta\Gamma_{hhh} = \frac{\Gamma_{hhh}^{loop} + \delta\Gamma_{hhh}^{loop} - \Gamma_{hhh}^{tree}}{\Gamma_{hhh}^{tree}} \quad (31)$$

where the coupling $\Gamma_{hhh}^{tree} = -3m_h^2/v$ represents the trilinear coupling at tree level.

By considering the degenerate case where $100 \text{ GeV} \leq m_\Phi \leq 500 \text{ GeV}$, a random scan over the IDM parameter space is performed taking into account the effects of the ATLAS

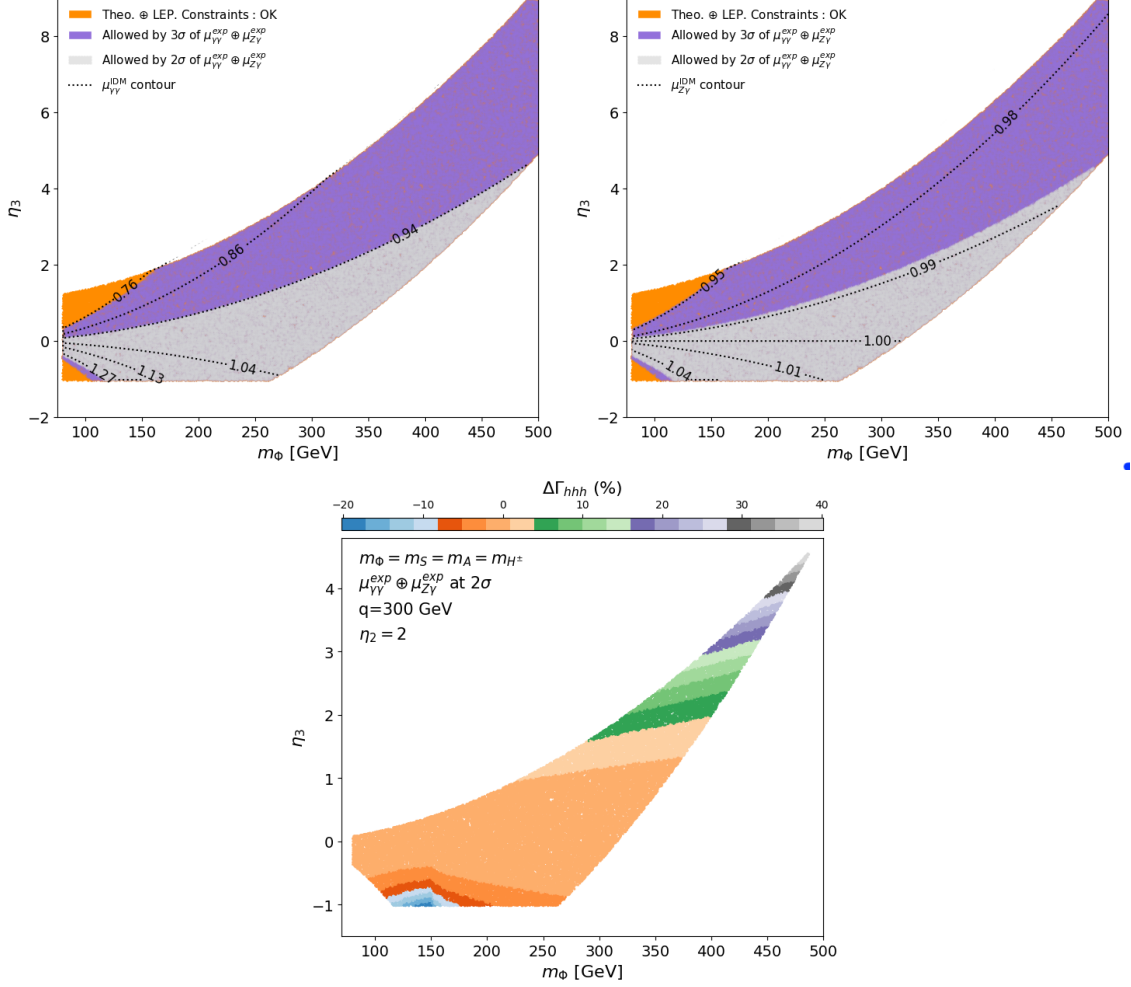


FIG. 4. Upper panel: correlation between $m_\phi = m_S = m_A = m_{H^\pm}$ and η_3 with the dot-dashed line corresponds to the $\mu_{\gamma\gamma}^{\text{IDM}}$ (left) and $\mu_{Z\gamma}^{\text{IDM}}$ (right) contours. Lower panel: the $\Delta\Gamma_{hhh}$ variation within the $(\eta_3 - m_\phi)$ plane at 95% .C.L. We set $\eta_2 = 2$.

and CMS experimental measurement constraints on $\mu_{\gamma\gamma, Z\gamma}$ at 95% C.L.. The upper panel of Figure.4 shows the allowed parameter space in the $(\eta_3 - m_\phi)$ plane with $\eta_2 = 2$. Thus, in addition to all the theoretical requirements, it further seem to point to the fact that at 99% C.L. of $\mu_{\gamma\gamma, Z\gamma}^{\text{exp}}$ measurements; the permissible space parameter requires $m_\phi \lesssim 500$ GeV and $\eta_3 \lesssim 9$ as reflected by the gray region. Nevertheless, scaling down to $\pm 2\sigma$ provides a reduced surface area (orange) with an upper limit can extend to 488 GeV, but still ruling out any enhancement for the $\text{Br}(h \rightarrow Z\gamma)/\text{SM}$ and $\text{Br}(h \rightarrow \gamma\gamma)/\text{SM}$ above 4.5% and 27%, respectively. However, it should further be emphasized that such experimental measurements require a positive value of μ_{22}^2 in order to validate the values in Eqs.(22-23-24).

The lower panel of Figure.4 addresses only the consistent points with $\mu_{Z\gamma,\gamma\gamma}^{exp}$ at 2σ C.L., and depicts the relative corrections to the triple coupling hhh in the $(\eta_3 - m_\Phi)$ plane, with the assumption that $q = 300$ GeV. At first sight, one can see how the space shrank so drastically compared to [33, 34] results, and the enhancement they found for the radiative corrections went down dozens of times, and had narrowed to only -20% for low m_Φ and 36% for m_Φ around 485 GeV. Furthermore, it is clear that the $|\Delta\Gamma_{hhh}|$ goes up steadily over η_3 for fixed value of m_Φ , and could reach its maximum around $\eta_3 = -1$ (around $\mu_{22}^2 \approx 50000 \text{ GeV}^2$) for $m_\Phi \approx 150$ GeV. Such latter point is amplified by the threshold channel $h^* \rightarrow \Phi\Phi$ that is open, where the momentum of the off shell Higgs boson is $q = 2m_\Phi = 300$ GeV.

B. Invisible Higgs decay and $\Delta\Gamma_{hhh}$

A further advantage of IDM enables to explain the invisible Higgs sector as it embeds S or A , both of which can be considered as stable WIMP particles, and then the SM Higgs can invisibly decay into $h \rightarrow SS$ or $h \rightarrow AA$ which can modify the total width of the Higgs boson and have significant impact on the LHC results. There exist several studies on the limit of the invisible decay of the SM Higgs boson, conducted by both ATLAS and CMS [35, 36]. The most recent limit, as reported by ATLAS in [37], reads:

$$\text{Br}_{\text{inv}} < 11\% \text{ at } 95\% \text{ C.L.} \quad (32)$$

and will be applied. The partial width for the process in Eq.(32) is expressed by,

$$\Gamma(h \rightarrow SS, AA) = \frac{v^2 \eta_{L,S}^2}{8\pi m_h} \cdot \sqrt{1 - \frac{4m_{S,A}^2}{m_h^2}} \quad (33)$$

and is proportional to $\eta_{L,S}^2$ given in Eq.(7).

Subsequently, as one of our aims through this study is to shed light on how far $\mu_{Z\gamma,\gamma\gamma}^{exp}$ together with other Higgs observable issues and the radiative corrections $\Delta\Gamma_{hhh}$ can examine the hidden sector within the IDM if the inert particle S is light enough, we have slightly changed our set of parameters to be

$$\begin{aligned} m_h &= 125.09 \text{ GeV}, \quad m_S \in [10, 62.5] \text{ GeV}, \quad m_A, m_{H^\pm} \in [80, 500] \text{ GeV}, \\ \eta_2 &= 2, \quad \mu_{22}^2 \in [-4 \times 10^4, 10^5] \text{ GeV}^2 \end{aligned} \quad (34)$$

In Figure.5, we show results for $\mu_{\gamma\gamma}$ (left) and $\mu_{Z\gamma}$ (right) as a function of η_3 . The invisible decay result is given by the color coding, while the solid, dotted and dashed black lines in

the left indicate the expected values at 2σ and 3σ on the $\mu_{\gamma\gamma}$ from HL-LHC [22] and ATLAS collaboration [19]. For $\mu_{Z\gamma}$, we note that our findings remain above the $-2\sigma = 0.6$ (0.54) CMS (HL-LHC) values (which are outside the plots) and close to the unity. At first glance, we can observe that the BSM deviation approaches a plateau as η_3 increases either for $\mu_{\gamma\gamma}$ or $\mu_{Z\gamma}$. This behavior can be explained by the destructive interference between the charged scalar and SM contribution. Regarding the branching ratio Br_{inv} , it remains mostly below the aforementioned recent limit if we consider either the $\mu_{Z\gamma}^{\text{CMS}}$ or $\mu_{\gamma\gamma}^{\text{ATLAS}}$ at 95% C.L.. However, the situation is drastically modified, and the Br_{inv} does not exceed one 1% if the $\mu_{\gamma\gamma}^{\text{HL-LHC}}$ at 95% C.L. is considered. Such branching ratio get suppressed for small values of $\eta_3 \sim 0$ (or $m_{H^\pm} \sim 80$ GeV).

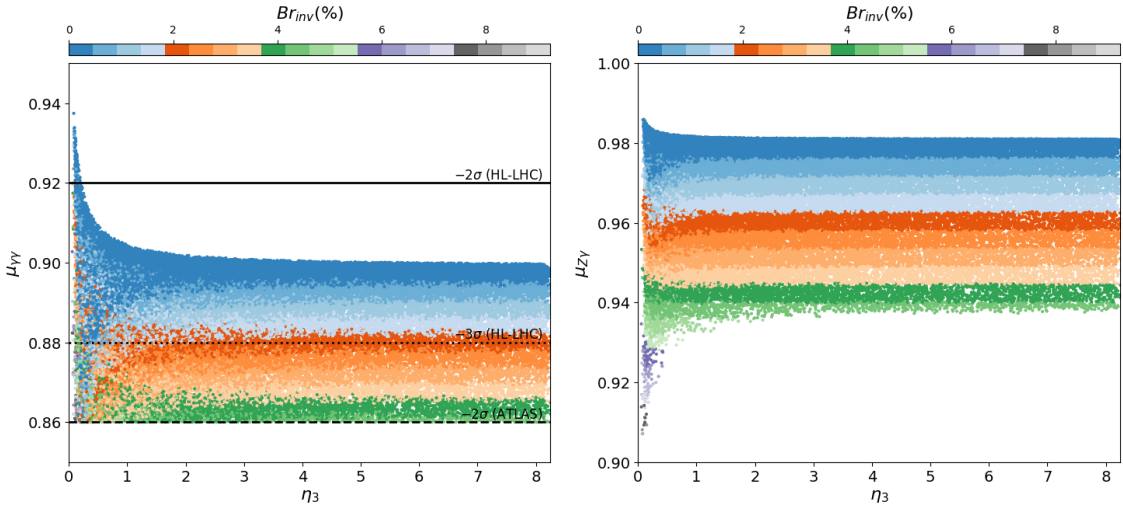


FIG. 5. The $\mu_{\gamma\gamma}$ (left) and $\mu_{Z\gamma}$ (right) as a function of η_3 in the quasi-degenerate case, with the color coding shows the invisible branching ratio. For both plots η_3 is fixed to be 2 and $10 \text{ GeV} \leq m_S \leq 62.5 \text{ GeV}$. The solid, dotted and dashed black lines in the left panel correspond to the more conservative limit from LHC-HL at -2σ , -3σ and ATLAS at -2σ , respectively.

In this regard, Figure.6 exhibits two possible connection between radiative corrections and the trilinear coupling η_3 in the presence of an invisible decay mode of h_{125} . A sizeable rate of the radiative corrections shows its ongoing reliance on the charged scalar bosons loops. Nevertheless, it should be emphasized that at 2σ of $\mu_{\gamma\gamma}^{\text{exp}}$, the Higgs invisible decay scenario is completely ruled out and no significant evidence can be proven. But as a byproduct of our analysis, stretching towards 3σ provides a likelihood, even the slightest. So, based on the relevant foregoing analysis, it is clearly seen from the left panel in Figure.6 that radiative

corrections could not exceed 63% at 95% C.L. at the HL-LHC, expecting an upper limit on the quartic coupling $\eta_3 \lesssim 0.35$. To achieve this, a light charged scalar boson, i.e $m_{H^\pm} \lesssim 100$ GeV, is needed. Nevertheless, such correction becomes almost entirely suppressed if the A and H^\pm are degenerated as can be drawn from right side in Figure.6.

C. Dark matter search

In this section, we consider the implication of $\mu_{\gamma\gamma}^{exp}$ measurement on the dark matter within the IDM. Such mysterious stuff that fills the universe may be detected either indirectly through looking for the products of dark matter interactions, especially the SM ones namely bosons, quarks and leptons [38, 39], or directly via interaction with ordinary matter by [40]. In our study, we focus on the latter and assume that the inert scalar boson S , is considered as good candidate to address this fundamental issue. The Feynman diagram describing the scattering between S and nucleon mediated by the observed $h = h_{125}$ is given by Figure.7

Additionally, the spin-independent scattering cross-section relevant to this process can be expressed by

$$\sigma_{SI} = \frac{\eta_L^2 f^2}{4\pi} \frac{\mu^2 m_N^2}{m_h^4 m_S^2} \quad (35)$$

where $f = 0.32$ [45], m_N and $\mu = m_N m_S / (m_N + m_S)$ denote respectively the Higgs-nucleon

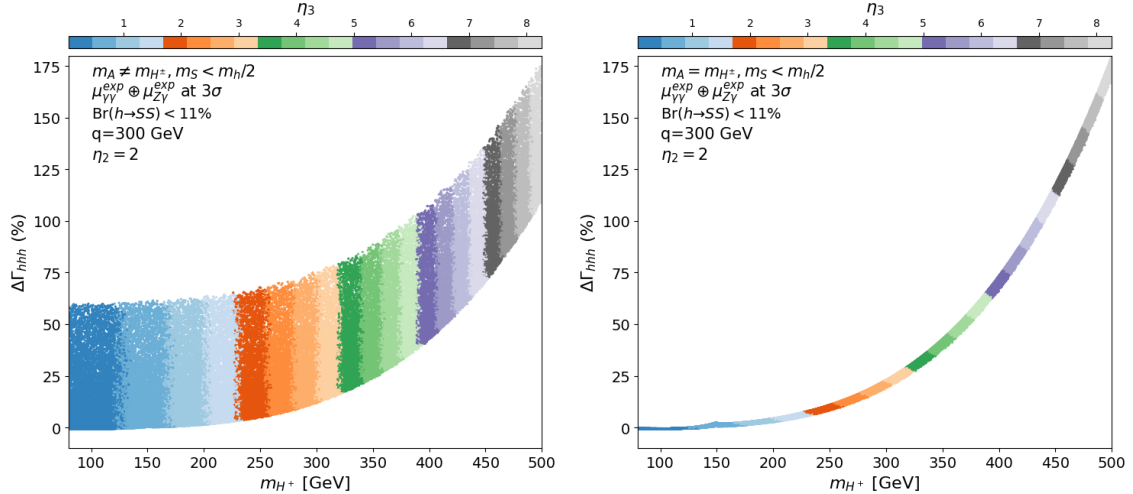


FIG. 6. Variation of the $\Delta\Gamma_{hhh}$ in the (m_{H^\pm}, η_3) plane for both cases : $80 \text{ GeV} \leq m_A, m_{H^\pm} \leq 500 \text{ GeV}$ (left) and $80 \text{ GeV} \leq m_A = m_{H^\pm} \leq 500 \text{ GeV}$ (right). We set for both : $m_S < m_h/2$, $q = 300 \text{ GeV}$ and $\eta_2 = 2$.

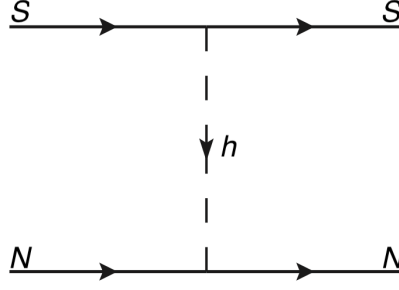


FIG. 7. Feynman diagram for the elastic spin-independent scattering cross section of Dark Matter with nucleon mediated by the SM-like Higgs h in the IDM

coupling, the nucleon mass and the reduced mass of dark matter and nucleon.

Figure.8 delimits the achievable points of space parameter for the Higgs-portal DM particle, S in the IDM. In generating this plot, further constraints are applied, in addition to those detailed in section II B, by imposing an upper limit on the DM relic density, $\Omega_{DM} h^2 \leq 0.12$ [46], calculated using the micrOMEGAs 5.2 framework [47]. We have also imposed: $\lambda_2 = 2$ as for previous plots and $\text{Br}_{\text{inv}} < 11\%$ while the inert scalar mass has been varied (in GeV)

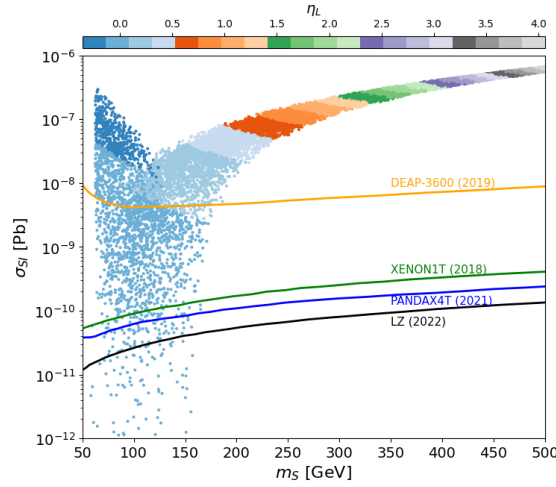


FIG. 8. Variation of the spin-independent cross section σ_{SI} with dark matter mass m_S where the color coding shows the variation of the η_L coupling. The DEAP-3600 [41], XENON1T [42], PandaX-4T [43], and LZ [44] resulting 90% C.L. upper limits are shown. Our parameters have been set in the non-degenerate case with $\lambda_2 = 2$.

in the range $[50, 500]$. The first thing to note is that Higgs–DM mass whether light (i.e. $M_S \leq 60$ GeV, which requires $|\eta_L| \leq 0.02$) or wedged in $[60, 180]$ (GeV), could be probed by the Xenon1T [42] experimental sensitivity bands, and its distribution fundamentally shifted in the PandaX-4T experiment and LZ [44]. However, there is still a narrow regions that are ruled out by those present experiments e.g.

i) the window with $m_h/2 \leq m_S/\text{GeV} \leq 135$ with $\mu_{22}^2 \leq 2.5 \text{ GeV}^2$ and $\eta_L \leq 0$.

ii) Also, the region where $m_S/\text{GeV} \geq 175$ together with $\eta_L \geq 0.25$,

but they are still under experimental scrutiny and might be tested in future experiences [48] widening an enough space parameters.

V. CONCLUSION

We have revisited in this paper the IDM as extension BSM by examining the two decay modes $\gamma\gamma$ and $Z\gamma$. In line with the actual data on the corresponding signal strengths $\mu_{\gamma\gamma}^{exp}$ and $\mu_{Z\gamma}^{exp}$, a particular focus is made on the implications of such measurements over many physical observables. Our results have shown that $\mu_{\gamma\gamma}^{exp}$ may clamp down the allowed space parameter for the IDM. Notably, at 2σ of $\mu_{\gamma\gamma}^{exp}$, the possibility of a Higgs invisible decay scenario is unequivocally excluded, leaving no substantial evidence to support it. This result highlights the stringent limits that current experimental data impose on alternative Higgs decay channels. As we have demonstrated, the dark matter had a foothold in this paper, and it is highly sensitive to the $\mu_{\gamma\gamma}^{exp}$ measurement. The corresponding cross section has been evaluated, and besides posing a challenge to detect the DM in the universe, it may also provide a way to constrain some model parameters.

-
- [1] S. Chatrchyan et al. (CMS), Observation of a new boson at a mass of 125 GeV with the CMS experiment at the LHC, *Phys. Lett.* **B716**, 30 (2012), [arXiv:1207.7235 \[hep-ex\]](#).
 - [2] G. Aad et al. (ATLAS), Observation of a new particle in the search for the Standard Model Higgs boson with the ATLAS detector at the LHC, *Phys. Lett.* **B716**, 1 (2012), [arXiv:1207.7214 \[hep-ex\]](#).

- [3] N. G. Deshpande and E. Ma, Pattern of symmetry breaking with two higgs doublets, [Phys. Rev. D **18**, 2574 \(1978\)](#).
- [4] Q.-H. Cao, E. Ma, and G. Rajasekaran, Observing the dark scalar doublet and its impact on the standard-model higgs boson at colliders, [Phys. Rev. D **76**, 095011 \(2007\)](#).
- [5] R. Barbieri, L. J. Hall, and V. S. Rychkov, Improved naturalness with a heavy higgs boson: An alternative road to cern lh physics, [Phys. Rev. D **74**, 015007 \(2006\)](#).
- [6] L. Lopez Honorez and C. E. Yaguna, The inert doublet model of dark matter revisited, [JHEP **09**, 046, arXiv:1003.3125 \[hep-ph\]](#).
- [7] E. M. Dolle and S. Su, The Inert Dark Matter, [Phys. Rev. D **80**, 055012 \(2009\)](#), [arXiv:0906.1609 \[hep-ph\]](#).
- [8] A. G. Akeroyd, A. Arhrib, and E.-M. Naimi, Note on tree level unitarity in the general two Higgs doublet model, [Phys. Lett. B **490**, 119 \(2000\)](#), [arXiv:hep-ph/0006035](#).
- [9] I. F. Ginzburg, K. A. Kanishev, M. Krawczyk, and D. Sokolowska, Evolution of Universe to the present inert phase, [Phys. Rev. D **82**, 123533 \(2010\)](#), [arXiv:1009.4593 \[hep-ph\]](#).
- [10] M. E. Peskin and T. Takeuchi, Estimation of oblique electroweak corrections, [Phys. Rev. D **46**, 381 \(1992\)](#).
- [11] R. L. Workman et al. (Particle Data Group), Review of Particle Physics, [PTEP **2022**, 083C01 \(2022\)](#).
- [12] A. Belyaev, G. Cacciapaglia, I. P. Ivanov, F. Rojas-Abatte, and M. Thomas, Anatomy of the Inert Two Higgs Doublet Model in the light of the LHC and non-LHC Dark Matter Searches, [Phys. Rev. D **97**, 035011 \(2018\)](#), [arXiv:1612.00511 \[hep-ph\]](#).
- [13] D. Dercks and T. Robens, Constraining the Inert Doublet Model using Vector Boson Fusion, [Eur. Phys. J. C **79**, 924 \(2019\)](#), [arXiv:1812.07913 \[hep-ph\]](#).
- [14] A. Ilnicka, M. Krawczyk, and T. Robens, Inert Doublet Model in light of LHC Run I and astrophysical data, [Phys. Rev. D **93**, 055026 \(2016\)](#), [arXiv:1508.01671 \[hep-ph\]](#).
- [15] M. Aaboud et al. (ATLAS), Search for the standard model Higgs boson produced in association with top quarks and decaying into a $b\bar{b}$ pair in pp collisions at $\sqrt{s} = 13$ TeV with the ATLAS detector, [Phys. Rev. D **97**, 072016 \(2018\)](#), [arXiv:1712.08895 \[hep-ex\]](#).
- [16] A. M. Sirunyan et al. (CMS), Search for invisible decays of a Higgs boson produced through vector boson fusion in proton-proton collisions at $\sqrt{s} = 13$ TeV, [Phys. Lett. B **793**, 520 \(2019\)](#), [arXiv:1809.05937 \[hep-ex\]](#).

- [17] G. Bélanger, B. Dumont, A. Goudelis, B. Herrmann, S. Kraml, and D. Sengupta, Dipole constraints in the inert doublet model from run 1 of the LHC, *Physical Review D* **91**, [10.1103/physrevd.91.115011](#) (2015).
- [18] E. Lundström, M. Gustafsson, and J. Edsjö, Inert doublet model and LEP II limits, *Physical Review D* **79**, [10.1103/physrevd.79.035013](#) (2009).
- [19] G. Aad *et al.* (ATLAS), Measurement of the properties of Higgs boson production at $\sqrt{s} = 13$ TeV in the $H \rightarrow \gamma\gamma$ channel using 139 fb $^{-1}$ of pp collision data with the ATLAS experiment, *JHEP* **07**, 088, [arXiv:2207.00348 \[hep-ex\]](#).
- [20] A. M. Sirunyan *et al.* (CMS), Measurements of Higgs boson production cross sections and couplings in the diphoton decay channel at $\sqrt{s} = 13$ TeV, *JHEP* **07**, 027, [arXiv:2103.06956 \[hep-ex\]](#).
- [21] A. Tumasyan *et al.* (CMS), Search for Higgs boson decays to a Z boson and a photon in proton-proton collisions at $\sqrt{s} = 13$ TeV, *JHEP* **05**, 233, [arXiv:2204.12945 \[hep-ex\]](#).
- [22] M. Cepeda *et al.*, Report from Working Group 2: Higgs Physics at the HL-LHC and HE-LHC, *CERN Yellow Rep. Monogr.* **7**, 221 (2019), [arXiv:1902.00134 \[hep-ph\]](#).
- [23] Evidence for the Higgs boson decay to a Z boson and a photon at the LHC, (2023).
- [24] J. F. Gunion, H. E. Haber, G. L. Kane, and S. Dawson, *The Higgs Hunter's Guide*, Vol. 80 (2000).
- [25] A. Djouadi, The Anatomy of electro-weak symmetry breaking. I: The Higgs boson in the standard model, *Phys. Rept.* **457**, 1 (2008), [arXiv:hep-ph/0503172](#).
- [26] A. Djouadi, The Anatomy of electro-weak symmetry breaking. II. The Higgs bosons in the minimal supersymmetric model, *Phys. Rept.* **459**, 1 (2008), [arXiv:hep-ph/0503173](#).
- [27] M. Krawczyk, D. Sokołowska, P. Swaczyna, and B. Świeżewska, Higgs $\rightarrow \gamma\gamma$, $Z\gamma$ in the Inert Doublet Model, *Acta Phys. Polon. B* **44**, 2163 (2013), [arXiv:1309.7880 \[hep-ph\]](#).
- [28] E. C. F. S. Fortes, A. C. B. Machado, J. Montaña, and V. Pleitez, Prediction of $h \rightarrow \gamma Z$ from $h \rightarrow \gamma\gamma$ at LHC for the IMDS₃ Model, *J. Phys. G* **42**, 115001 (2015), [arXiv:1408.0780 \[hep-ph\]](#).
- [29] G. Passarino and M. J. G. Veltman, One Loop Corrections for e $^+$ e $^-$ Annihilation Into mu $^+$ mu $^-$ in the Weinberg Model, *Nucl. Phys. B* **160**, 151 (1979).
- [30] M. Aiko, J. Braathen, and S. Kanemura, Leading two-loop corrections to the Higgs di-photon decay in the Inert Doublet Model, (2023), [arXiv:2307.14976 \[hep-ph\]](#).

- [31] W. Hollik and S. Penaranda, Yukawa coupling quantum corrections to the selfcouplings of the lightest MSSM Higgs boson, [*Eur. Phys. J. C* **23**, 163 \(2002\)](#), [arXiv:hep-ph/0108245](#).
- [32] S. Kanemura, Y. Okada, E. Senaha, and C. P. Yuan, Higgs coupling constants as a probe of new physics, [*Phys. Rev. D* **70**, 115002 \(2004\)](#), [arXiv:hep-ph/0408364](#).
- [33] A. Arhrib, R. Benbrik, J. El Falaki, and A. Jueid, Radiative corrections to the Triple Higgs Coupling in the Inert Higgs Doublet Model, [*JHEP* **12**, 007](#), [arXiv:1507.03630 \[hep-ph\]](#).
- [34] J. E. Falaki, Revisiting one-loop corrections to the trilinear Higgs boson self-coupling in the inert doublet model, [*Phys. Lett. B* **840**, 137879 \(2023\)](#), [arXiv:2301.13773 \[hep-ph\]](#).
- [35] Combination of searches for invisible Higgs boson decays with the ATLAS experiment, (2020).
- [36] A. Tumasyan et al. (CMS), Search for invisible decays of the Higgs boson produced via vector boson fusion in proton-proton collisions at $s=13$ TeV, [*Phys. Rev. D* **105**, 092007 \(2022\)](#), [arXiv:2201.11585 \[hep-ex\]](#).
- [37] Combination of searches for invisible decays of the Higgs boson using 139 fb⁻¹ of proton-proton collision data at $s=13$ TeV collected with the ATLAS experiment, [*Phys. Lett. B* **842**, 137963 \(2023\)](#), [arXiv:2301.10731 \[hep-ex\]](#).
- [38] J. L. Feng, Dark Matter Candidates from Particle Physics and Methods of Detection, [*Ann. Rev. Astron. Astrophys.* **48**, 495 \(2010\)](#), [arXiv:1003.0904 \[astro-ph.CO\]](#).
- [39] D. Hooper, Particle Dark Matter, in [Theoretical Advanced Study Institute in Elementary Particle Physics: T](#) (2010) pp. 709–764, [arXiv:0901.4090 \[hep-ph\]](#).
- [40] K. J. Bae, Reconsidering the Blind Spots of Neutralino Dark Matter: a Perturbative Approach, [*New Phys. Sae Mulli* **72**, 573 \(2022\)](#).
- [41] P. A. Amaudruz et al. (DEAP-3600), First results from the DEAP-3600 dark matter search with argon at SNOLAB, [*Phys. Rev. Lett.* **121**, 071801 \(2018\)](#), [arXiv:1707.08042 \[astro-ph.CO\]](#).
- [42] E. Aprile et al. (XENON), Dark Matter Search Results from a One Ton-Year Exposure of XENON1T, [*Phys. Rev. Lett.* **121**, 111302 \(2018\)](#), [arXiv:1805.12562 \[astro-ph.CO\]](#).
- [43] Y. Meng et al. (PandaX-4T), Dark Matter Search Results from the PandaX-4T Commissioning Run, [*Phys. Rev. Lett.* **127**, 261802 \(2021\)](#), [arXiv:2107.13438 \[hep-ex\]](#).
- [44] J. Aalbers et al. (LZ), First Dark Matter Search Results from the LUX-ZEPLIN (LZ) Experiment, (2022), [arXiv:2207.03764 \[hep-ex\]](#).
- [45] J. Giedt, A. W. Thomas, and R. D. Young, Dark matter, the CMSSM and lattice QCD, [*Phys. Rev. Lett.* **103**, 201802 \(2009\)](#), [arXiv:0907.4177 \[hep-ph\]](#).

- [46] P. A. Zyla et al. (Particle Data Group), Review of Particle Physics, [PTEP **2020**, 083C01 \(2020\)](#).
- [47] G. Belanger, A. Mjallal, and A. Pukhov, Recasting direct detection limits within micrOMEGAs and implication for non-standard Dark Matter scenarios, [Eur. Phys. J. C **81**, 239 \(2021\)](#), [arXiv:2003.08621 \[hep-ph\]](#).
- [48] J. Aalbers et al. (DARWIN), DARWIN: towards the ultimate dark matter detector, [JCAP **11**, 017, arXiv:1606.07001 \[astro-ph.IM\]](#).